



EFFECTS OF NATURE-INSPIRED METHODS ON THE EFFICIENCY OF THE FLOW PART ELEMENTS OF HYDRAULIC MACHINES

Aleksander Volkov, Artem Ryzhenkov, Aleksey Druzhinin, German Kromm and Nadezhda Panferova
National Research University Moscow Power Engineering Institute, Moscow, Russia
E-Mail: grigoriev.srcw@gmail.com

ABSTRACT

Hydraulic machine is one of the most widespread technical systems in various areas of production. The paper examines the problem of the efficiency of vane hydraulic machines and ways to address it through the biomimetic approach. The study reviews previous research into the peculiarities of the construction of living organisms that provide a reduction of their energy costs. The hydrodynamic effect of the sharkskin structure is created by the roughnesses (micro ribs) oriented along the flow and allows reducing the value of hydraulic drag in the near-wall area. Hypotheses are proposed about the possibilities of applying these features and approaches in technical systems, particularly for flow part elements of hydraulic machines. The authors set the goal to assess the efficiency of using an imitation of sharkskin in a simplified form of scales, and geometric outgrowths, which will provide the necessary hydrodynamic effect. The development includes 3D modeling and subsequent computational verification on the surfaces of flow part elements of hydraulic machines. The findings enable conclusions on the effect of scale placement on the plate on energy losses as the plate is streamlined by fluid. A conclusion is drawn on the current state of the use of nature-inspired technology in hydromechanical engineering and the development trends in this field.

Keywords: energy saving, energy efficiency, environmentally friendly technology, hydropower, vane system.

Manuscript Received 11 December 2023; Revised 22 January 2024; Published 10 February 2024

INTRODUCTION

Vane hydraulic machines are among the most widespread technical systems today. Pydroelectric power stations produce about 18% of the energy in Russia (according to 2019 data) [1], and energy consumption to drive vane pumps amounts to 30% of the world's total energy production in 2019 [2]. This generates quite an urgent task of reducing energy losses in hydromachines in general and improving their overall efficiency in operation.

The energy conversion efficiency (ECE) of a vane hydromachine is an averaged integral estimate of mechanical, volumetric, and hydraulic losses. Mechanical losses are caused by drag in the bearing and sealing units of the hydraulic unit and friction between the fluid and the outer surfaces of the impeller disks. Volumetric losses refer to the amount of internal and external leakage of the working fluid through the sealing assemblies. Hydraulic losses define the amount of energy that is generally spent on vortex formation, local changes in flow direction and velocity, and hydraulic drag. The largest share of all losses in a vane machine is made up of hydraulic losses. For example, the hydraulic ECE of modern vane pumps ranges from 0.7 to 0.9, while the mechanical ECE ranges from 0.9 to 0.95 and the volumetric ECE is 0.97 [3]. Therefore, when developing new hydroelectric units or modernizing existing ones, it is of primary importance to address problems related to the reduction of hydraulic losses.

Most of the installed hydraulic units often operate in suboptimal modes, in which their efficiency is significantly reduced [4]. This results from several reasons, starting with suboptimal decisions when selecting a hydraulic machine to meet the requirements of the

consumer network, and ending with the regulation of operating modes and changes in the parameters of the hydraulic network, associated with the wear and tear of its elements [5]. For these reasons, hydraulic engineering is faced with the global challenge of extending the possible working range of both pumps and hydraulic turbines.

At present, a considerable number of methods are being developed to improve the efficiency of vane hydromachines [6-8]. Some examples include optimizing hydraulic unit operating modes and using modern computer-aided design systems together with neural networks when creating hydraulic machines [9]. Moreover, some engineering solutions can be developed based on some phenomena studied by other sciences. Thus, the application of biomimetics principles is a promising direction in the development of hydraulic engineering.

Biomimetics is a science investigating the properties, phenomena, and principles of living nature organization to create nature-like technologies and apply them in technical systems [10]. At present, the following effects, promising for hydraulic engineering, are intensively studied: the humpback whale fin effect, the lotus effect, the hydrodynamic effect of sharkskin, and the effect of the tail fin of some birds.

The present study focuses on the hydrodynamic effect of sharkskin. The hypothesis suggested is that the flow processes observed in the flow part of hydromachines are similar to the movements of sharks as the representatives of ichthyofauna in the aquatic environment.

To assess the state of research in biomimetics, specifically on the priority natural effects in the context of



the above-mentioned problems and tasks, we reviewed and systematized the results of research on the relevant topic with consideration of related areas.

LITERATURE REVIEW

Morphology and Mechanisms of the Sharkskin Effect

Sharkskin has long drawn human attention because of its rough texture. Today, biomimetic engineers are increasingly focused on it because sharkskin has several properties that help reduce hydraulic drag and protect against the formation of various biological deposits on its surface. However, there is an ongoing debate in the scientific community about the main mechanisms that contribute to the decrease in drag in the water.

The most interesting review of this issue is presented by S. Martin and B. Bhushan [11]. Their paper deals with the morphological features of sharkskin. In addition, the authors set themselves the task of assessing

the current state of research on sharkskin and describing the problems encountered when creating such a biomimetic surface.

Several companies and research institutes have developed artificial surfaces that replicate the structure of sharkskin. Yet upon closer inspection, according to the researchers, most of these surfaces either do not have or bear only a rough resemblance to sharkskin.

What distinguishes the shark from other fish is that its skin is not covered with a copious layer of mucus like other fast-swimming fish species, such as sailfish or tuna. Sharkskin does contain mucus cells, but in much smaller numbers, which does not allow the mucus to completely cover the finely scaly surface of the body. Nevertheless, the thin mucous layer between the scales seems to contribute to a more intense vortex formation on the shark's body (Figure-1) and causes a liquid rolling bearing effect [12].

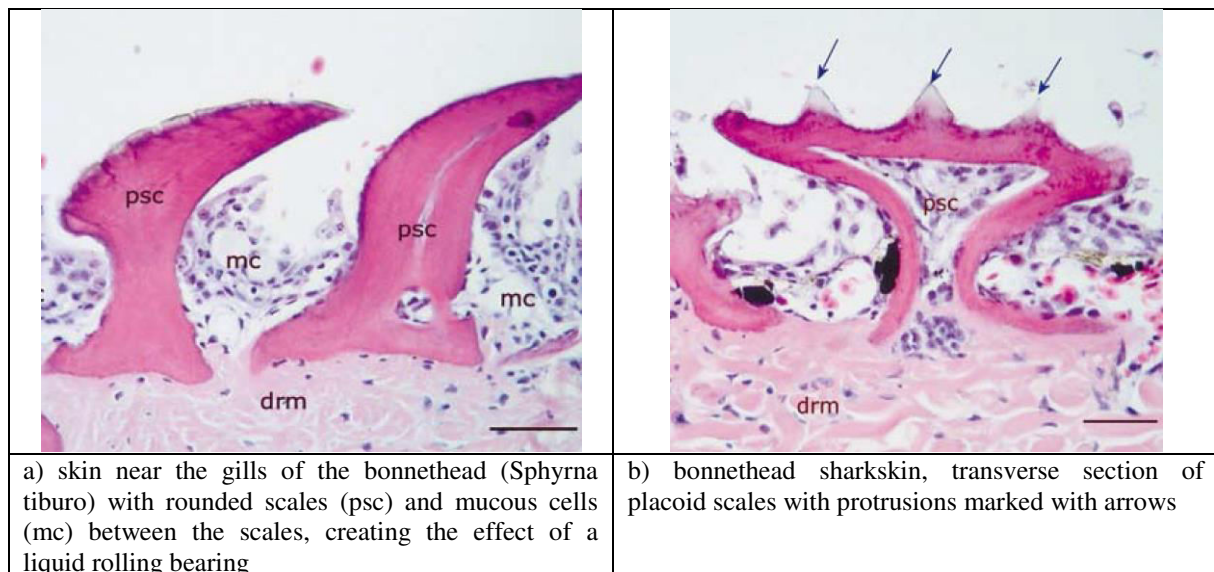


Figure-1. Structure of the fine scaly skin of the shark species *Sphyrna tiburo*. scale – 50 microns
 drm - derma, psc - placoid scale.

The scales of fast-swimming sharks have flat elements that overlap in varying degrees and are covered with sharp V-shaped ridges and rounded U-shaped depressions between them. The ridges are typically oriented along the axis of the body. Depending on size, each scale has three to seven ridges at intervals of 30 to 100 μm , with the spacing usually varying between shark species depending on the body area. In most of the 30 species that have been studied so far, this distance is less than 100 μm . Here it is important to note that fast-swimming sharks can move at speeds up to 10-20 m/s. It has been suggested that sharkskin interacts with the viscous sublayer of the turbulent boundary layer by forming a longitudinal flow separation. In earlier studies [13], several authors suggested that the reason for the supposed decrease in the drag of sharkskin was the maintenance and active modification of the laminar

boundary layer due to the presence of micro ribs in the longitudinal direction. This hypothesis has been confirmed by experimental studies of V-shaped ridges, which reduce resistance by up to 8% [14].

Apart from the research on the structure of scale surfaces with longitudinal ridges, it has become apparent that fast-swimming sharks can change the angle of their scales depending on their speed. In some species, the angle of scales is observed to change due to the growing tension of the skin with the increasing speed of movement. Studies have found that internal pressure increases more than tenfold in the transition from slow to fast swimming. The distance between the scales is slightly greater, but more important are the bristle scales, the angle of which can change up to 40° [15]. The ability to change the angle of the scales allows sharks to alter the nature of fluid flow around their bodies at higher swimming speeds,



preventing separation of currents and adapting the structure of the skin surface to the speed. Laboratory experiments of M.V. Ankhelyi, D.K. Wainwright, and G.V. Lauder [16] with ridges positioned perpendicular to the flow direction, simulating a bristle scale, detected the occurrence of vortices and a decrease in hydraulic drag. Subsequent studies investigated the bristle effect of sharkskin caused by the lifting of scales at different angles in detail. Engineers have attempted to create a replica of the skin of an adult shortfin mako shark (*Isurus oxyrinchus*) with scales that have bristles arranged perpendicular to the skin. The results of experimental studies simulating such a high angle of the bristles location confirm the formation of vortices inside the interscale cavities. The hypothesis proposed is that at low Reynolds numbers, the embedded vortices can reduce the hydraulic drag of surface friction because of the liquid rolling bearing effect. Mucus between the scales allows this drag-reducing effect to be maintained (Figure-1). Thus, these embedded vortices can act as a boundary layer control mechanism, delaying or even preventing flow detachment. A similar biomimetic effect is known in aerodynamics. One example of this is making dimples in a golf ball.

To replicate sharkskin, some researchers used the skin of dead sharks with the scales pressed down as a template to create hard organic glass samples and soft polydimethylsiloxane samples. Even this simplified sharkskin shows an 8.25% drag reduction effect in a water tunnel experiment. As mentioned above, other researchers have created models with extremely large scale angles (up to 90°), observing drag reduction effects as well. A point to note is that all the conditions in which sharks can change the characteristics of their skin depending on their speed are difficult to reconcile. In addition, the boundary layer of a moving shark is complex due to constant undulation and is certainly different from a layer on a rigid plate, such as a model with rigid plating or a structured hull surface.

Other reviewed publications also provide information on the morphology of sharkskin and the mechanisms responsible for reducing hydraulic drag. G.V. Lauder *et al.* [17] report experiments with shark scales placed on foil and a flexible membrane (Figure-2), which show a significant decrease in the drag on the incoming flow.

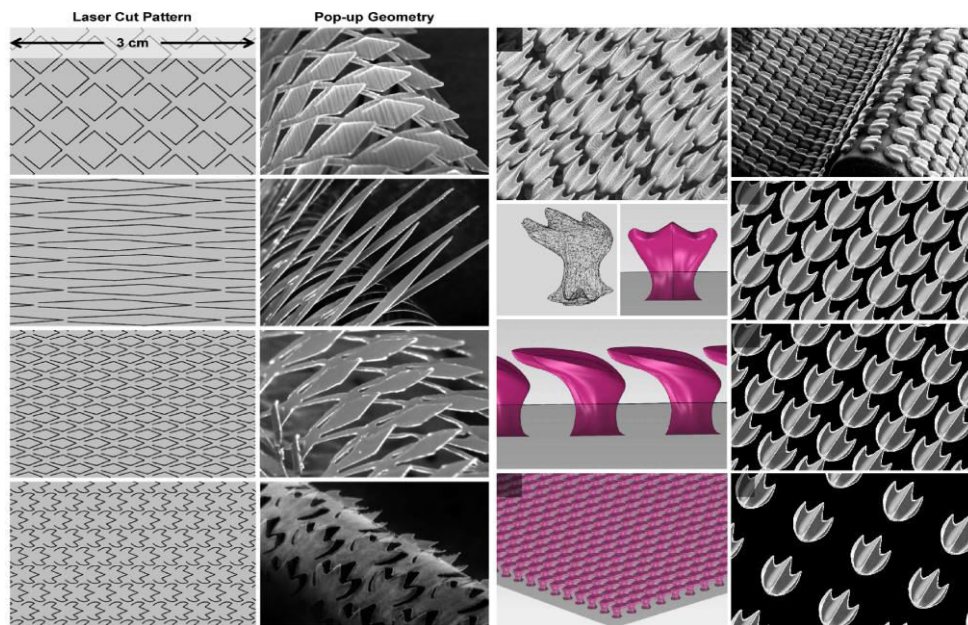


Figure-2. Different options for making foil and flexible membrane with sharkskin imitation.

Some bird species, such as skimmers, have a similar mechanism for reducing drag in a fluid environment as sharks do (Figure-3).

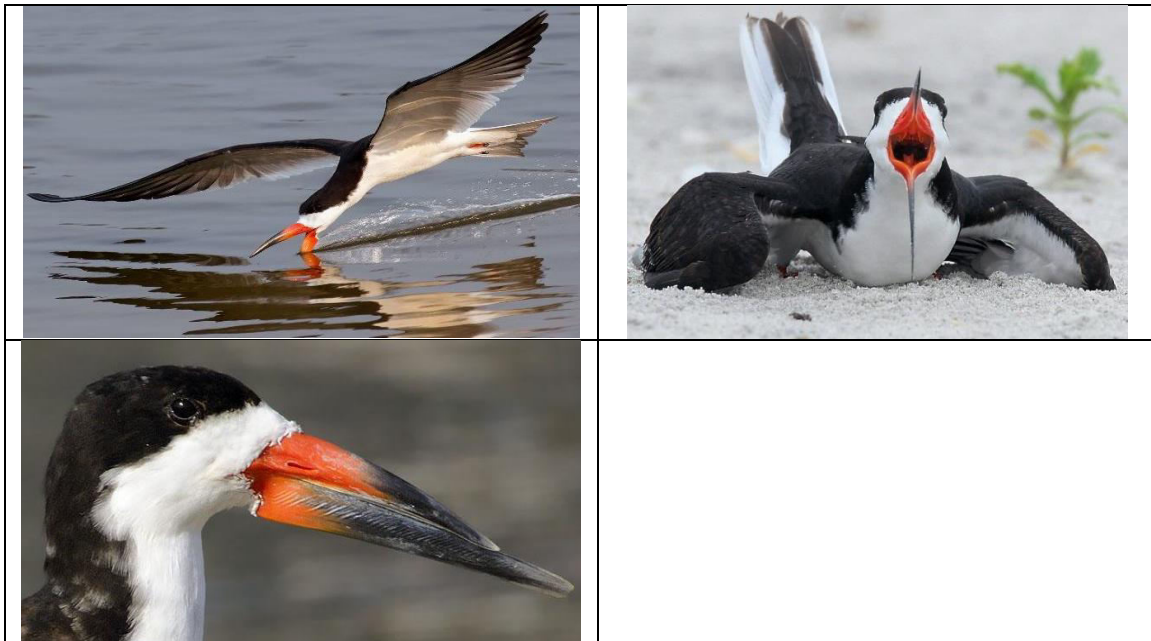


Figure-3. Structure of the lower beak of skimmers.

The lower beak of these birds, which is submerged in water when hunting, has a ribbed surface. Studies indicate that this structure of the beak changes the way fluid flows around its ribbed walls [18]. Scientific findings demonstrate that the reduction of hydraulic drag due to this natural modification ranges from 2.8 to 3.9%. This allows the bird to put less effort into the interaction of the beak with the water, increasing the efficiency of the hunt.

Replicating the Structure of Sharkskin and Optimizing its Models

Since engineers are quite interested in the study of sharkskin because of its properties to reduce hydraulic drag, it is a matter of no small importance to create and study models of sharkskin for use in technical systems.

X. Pu, G. Li, and H. Huang [19] produced a biomimetic shark using elastomer stamping techniques using polydimethylsiloxane. The surface microstructure (Figure-4) of the sharkskin was studied using scanning electron microscopy (SEM).

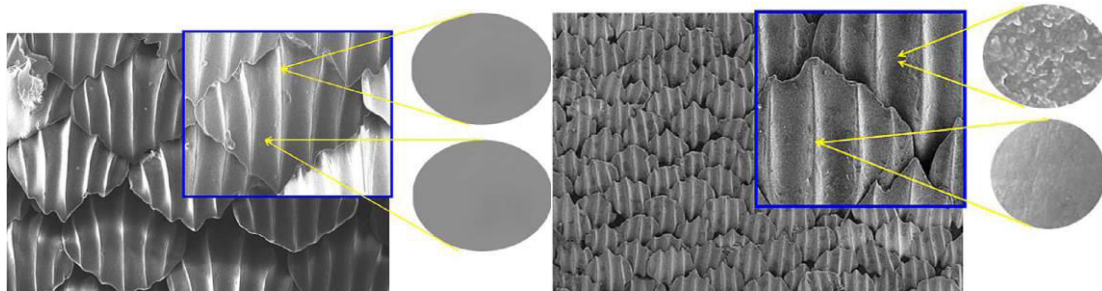
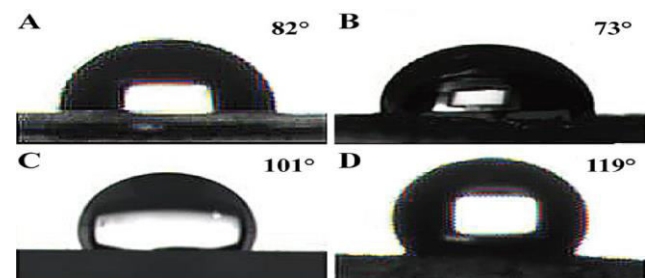


Figure-4. A study of the microstructure of sharkskin with SEM.

To analyze the hydrophobic mechanism of the sharkskin surface, we determined the effect of the biomimetic microstructure on surface wettability by measuring the angle of contact with water (Figure-5).



A, C – smooth surfaces; B, D – microstructured surfaces

Figure-5. Comparison of contact angles of different surfaces with water.



Additionally, several experiments were conducted to evaluate hydraulic drag. From the results, it was concluded that the biomimetic surface of sharkskin plays a significant role in the reduction of drag. The maximum drag reduction reached 12.5% compared to the smooth surface.

D. Chen *et al.* [20] described a biomimetic sharkskin surface that reduces hydraulic drag. A variety of methods for manufacturing surfaces with sharkskin morphology (Figure-6) and possible applications in fluid mechanics and hydraulics were also illustrated.

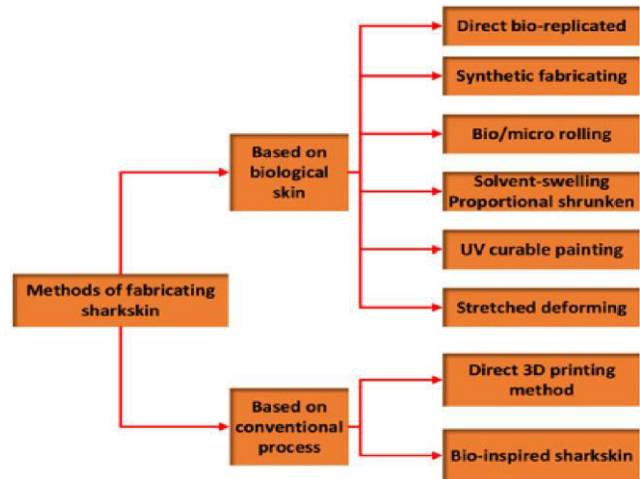


Figure-6. Methods for replicating a biomimetic surface based on sharkskin.

B. Daehne and B. Watermann [21] examined a high-precision replication of sharkskin consisting of filaments attached to microgrooves that mimic sharkskin. Pre-treated sharkskin was used as a casting template for making a flexible silicone rubber matrix by soft molding. Next, a water-based epoxy resin was used to graft long chains that reduce resistance and make synthetic sharkskin with realistic microgrooves (Figure-7).

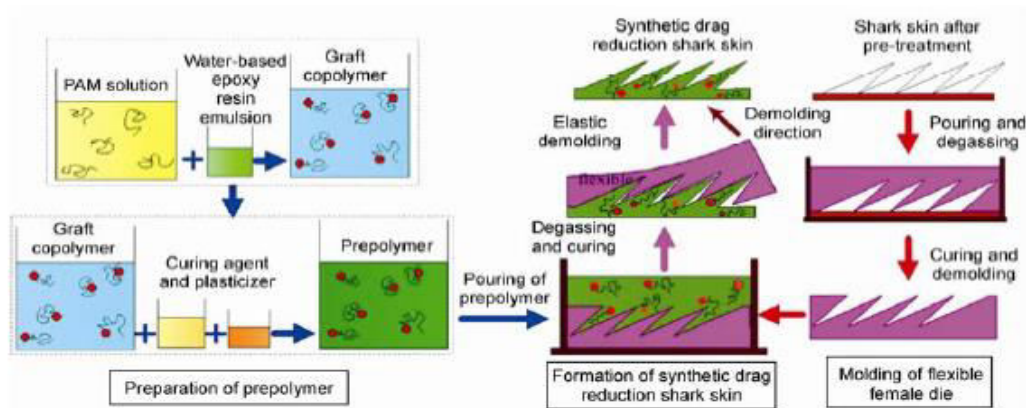


Figure-7. The process of creating a synthetic replica of sharkskin.

Hydraulic drag reduction experiments show that the material has a superior synthetic drag reduction effect with a maximum drag reduction factor of up to 24.6% at the tested speeds (Figure-8).

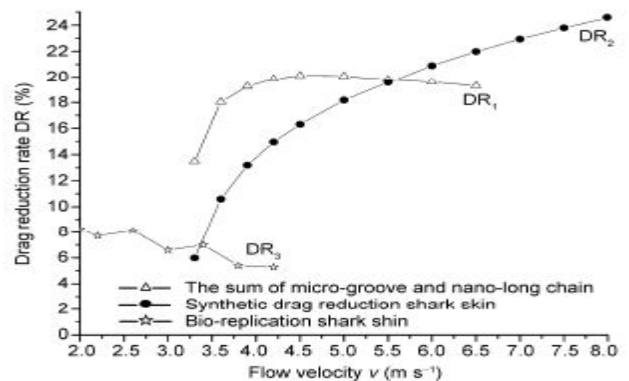


Figure-8. Diagram of hydraulic drag reduction as a function of flow velocity.



L. Wen, J. C. Weaver, and G. V. Lauder [22] present a study of the geometry, fabrication methods, and hydrodynamic tests of a synthetic flexible membrane made of sharkskin. A 3D model of sharkskin ridges was constructed using images of the skin of the shortfin mako (*Isurus oxyrinchus*). Using 3D printing, thousands of rigid synthetic shark scales were placed on flexible membranes in a given linear order. This flexible 3D-printed sharkskin model was then tested in the water using a robotic oscillating device that either held the models in a stationary position or dynamically moved them at the speed of sharks' self-propelled swimming. Compared to the smooth control model without ridges, the sharkskin printed using additive technologies showed an increased moving speed with reduced energy consumption for certain movement modes. For example, at a frequency of 1.5 Hz and an amplitude of ± 1 cm, the movement speed increased by 6.6% and the energy consumption per movement decreased by 5.9%. The ability to manufacture synthetic biomimetic sharkskin opens up a wide range of possible manipulations with the surface roughness parameters and the possibility of studying the hydrodynamic consequences of different skin ridge shapes found in different shark species.

M.D. Ibrahim *et al.* [23] studied the reduction of drag on ships using a simplified sharkskin simulation. In this work, models were created using computer-aided design software and then computational fluid dynamic (CFD) simulation was performed to evaluate the hydrodynamic efficiency of sharkskin-based biomimetic surfaces. Interestingly, the quantitative results obtained indicate that the presence of biomimetic sharkskin applied to the hulls of ships gives a reduction of the drag coefficient by about 3.75%, as well as a reduction of 3.89% of the drag force experienced by the ships. Theoretically, since the drag force could be reduced, this could lead to a more efficient vessel with better cruising speed. This could have a greater impact on shipping or the maritime industry worldwide.

An interesting application of the hydrodynamic effect of sharkskin is presented by C. Liu *et al.* [24]. The purpose of this research was to place nature-like non-smooth structures at the bottom of tire tread grooves to improve aquaplaning performance without affecting other tire characteristics. A finite element model of the 185/60R15 tire was used, and its accuracy was verified by load testing on a CSS-88100 electronic tire tester. The fluid flow model was analyzed using CFD simulation. The simulated critical aquaplaning velocity corresponded to the velocity derived from the empirical formula of the NACA. Similar to the structure of sharkskin microribs, three types of non-smooth surfaces were used. In addition, the drag reduction rate, shear stress, and flow velocity distribution were compared for the different grooves. Then, an optimized non-smooth structure with the best drag reduction effect among the three surfaces was placed at the bottom of the longitudinal grooves of the nature-inspired tire. Simulation results show the bionic tire is reducing hydrodynamic lift. With these improvements, the nature-inspired tire significantly improved the critical

aquaplaning speed. The results of these studies can be implemented to improve aquaplaning performance without sacrificing other tire characteristics.

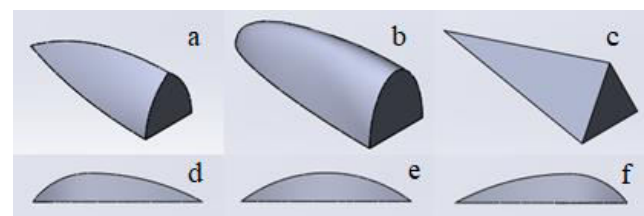
L. Wen *et al.* [25] and A.G. Domel *et al.* [26] present their findings on the effects of various geometric parameters of the biomimetic sharkskin on the resistance of a flexible membrane to motion. The researchers assessed the degree to which the flow was affected by the scale pattern, the distance between the scales, and the size of the elements. Our study, in turn, presents an imitation of sharkskin in a simplified form of scales represented by geometric growth using plates, which provide a similar hydrodynamic effect.

Drawing on the accumulated experience of researcher's worldwide dealing with the problem of biomimicry for technical systems, this study set out to develop a sharkskin simulation in a simplified form of scales represented by geometric growths that would achieve a similar hydrodynamic effect. To achieve this goal, computational and numerical verification was carried out on the surfaces of the flow part elements of hydraulic machines.

MATERIALS AND METHODS

Given the large number of possible shapes of outgrowths, the study was carried out using canonical regions, the flow around which is quite well studied. A plate was chosen as such an object in the first approximation.

Using 3D modeling software, models of plates and scales of several simple geometric shapes imitating sharkskin were created (Figure-9). The maximum height and width of the simulation element are 0.5 mm, while the length varies from 1.5 to 3 mm depending on the shape. The sharkskin modification was used on the upper side of the plate, where each scale was staggered against the other. The dimensions of the plate are: length 12 mm, width 2 mm, and thickness 1 mm. The degree of influence of these modifications was determined with the CFD simulation package, which relies on the finite-volume method [27].



a, b, c - scales without a shank end; d, e, f - with a shank

Figure-9. Imitation models of shark scales.

The calculated region for this problem is the area around the plate, in which the fluid flow is assessed. Given the need to consider the flow both in the boundary layer region and in the flow core, the following dimensions of the calculated region have been defined: 20 mm in front of the plate, 40 mm after, and 15 mm above and below the plate (Figure-10).

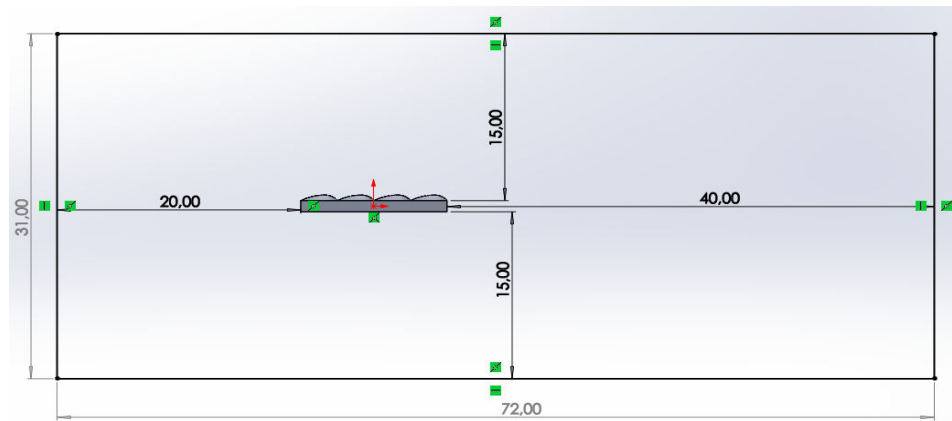


Figure-10. Dimensions of the investigated calculated flow area.

The construction and subdivision of the calculated domain into elements were performed automatically, given a crushed grid pattern near the wall. In the near-wall region, the grid is divided into prismatic elements, and in the main flow region - into tetrahedrons. The boundary layer grid was constructed using the Smooth Transition method with the following control values: Transition Ratio - 0.77; Maximum Layers - 5; Growth Rate - 1.2. An example of the subdivision of the calculated area into elements is presented in Figure-11.

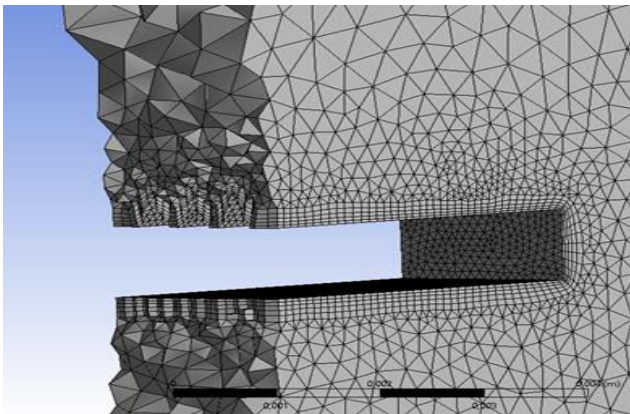


Figure-11. Appearance of the grid of control volumes of the calculated flow area.

The next step was to set the boundary conditions for the computer simulation of the Steady State streamline process. This process can be divided into two parts:

- boundary conditions that define the laws of variation of parameters on the boundaries of the calculated region;
- internal conditions that define the laws of change in the thermo-physical properties of the simulated medium (density, dynamic viscosity, heat capacity, etc.).

The medium chosen for the simulation from the standard library is water with the following parameters:

density - 997.05 kg/m³; dynamic viscosity coefficient - 0.89·10⁻³ Pa·s. The most universal for solving this problem is the shear stress transport (SST) model of turbulence. For each boundary surface, different conditions were specified (Table-1).

After generating the boundary conditions, the solution of the system of hydrodynamic equations consisting of the Navier-Stokes equation, the continuity equation, and the energy equation began immediately. The following calculation conditions were set: maximum number of iterations - 100; required accuracy - 1·10⁻⁴.

Table-1. Boundary conditions.

Inlet	
Velocity	1 or 10 m/s
Outlet	
Static pressure	0 Pa
Wall including the plate surface	
Movement condition	Motionless
Displacement condition	No slip (for viscous fluids)
Roughness	None
Symmetry condition on the sides of the calculated area	

To solve the research problem, an experimental plan aimed at analyzing the wake of a smooth plate was formed.

The computational method consisted of applying the momentum theorem for the known wake of a streamlined body. Thus, the resistance of the plate was determined, i.e., the relationship between the shear stress on the wall and the values of the displacement thickness and the thickness of the momentum loss:

$$\int_0^h \frac{\partial}{\partial x} [u(U_\infty - u)] dy + \frac{\partial U_\infty}{\partial x} \int_0^h (U_\infty - u) dy = \frac{\tau_0}{\rho} \quad (1)$$

where: u – local velocity, U_∞ – undisturbed flow velocity, h – calculation area boundary, ρ – density, τ_0 – shear



stress on the wall. The advantage of this expression is that it can be applied to both laminar and turbulent flows if time-averaged velocity components are used instead of instantaneous values.

The accuracy of the computational studies performed was assessed by verifying the computational results with a physical experiment on the streamlining of

the plate with a free flow of water. For this purpose, we used a hydrodynamic flume developed at the Moscow Power Engineering Institute National Research University (Moscow, Russia), which presents a frame construction with an open channel with transparent walls of 4,000 mm length and a rectangular section of 252 x 450 mm (Figure-12).

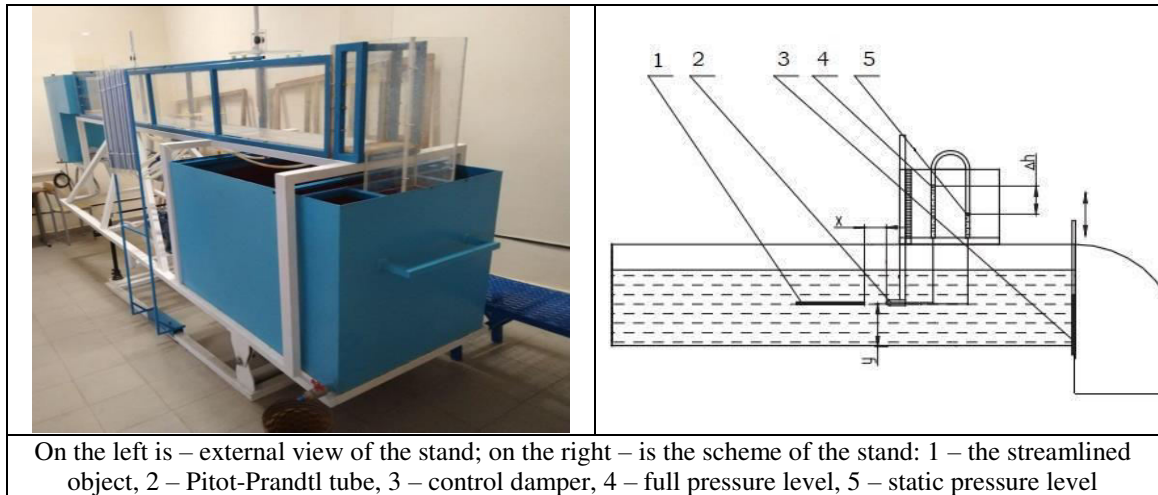


Figure-12. Hydrodynamic flume developed at the Moscow Power Engineering Institute National Research University for the study of open streams.

A 7.5 kW pump supplies water from the main fluid storage tank through a stilling guide unit. Regulation of the water flow rate in the canal is carried out by a frequency converter, while the level in the flume and the flow rate are regulated by two dampers 3 at the inlet and outlet of the flume. The maximum flow velocity of water in the channel does not exceed 1.5 m/s. Water returns from the flume to the main reservoir, from which it flows back to the pressure pipe.

RESULTS AND DISCUSSIONS

At the trailing edge of the plate, both velocity profiles in the boundary layers above and below the plate merge into one profile, forming a wake flow (Figure-13). The velocity difference of this flow in its central part decreases as it moves away from the plate and the width of the flow increases.

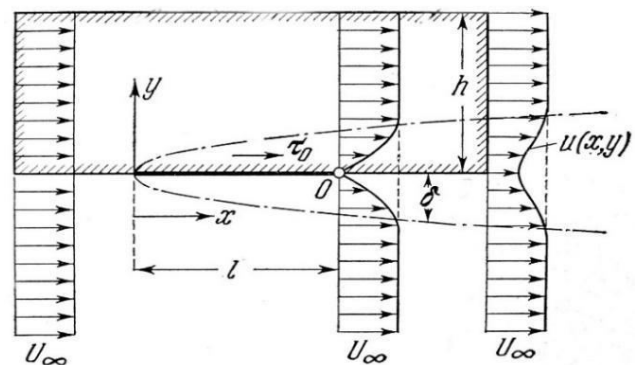


Figure-13. Wake behind the plate streamlined by the fluid.

The size of the depression in the wake flow velocity profile is directly related to the resistance of the body. However, the shape of the velocity profile at a large distance from the body is independent of its shape. In the immediate vicinity behind the body, the shape of the wake flow velocity profile is dictated by the boundary layer. Data on velocity distribution in the wake flow allow calculating the plate's resistance using the momentum theorem.

The results of the computational experiment were used to determine the full pressures at the inlet to the calculated area and the outlet from it. Based on the obtained results, we determined the pressure differential from the inlet to the outlet and using these calculated values - the pressure losses. All the data are summarized in Table-2.

**Table-2.** Estimation of pressure losses caused by flow around small plates.

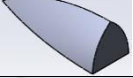






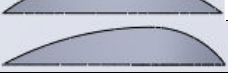
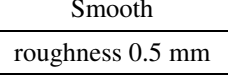
Sharkskin element shape/control plate type	Reynolds number	Full inlet pressure, Pa	Full outlet pressure, Pa	Pressure differential	
				Pa	%
Flow velocity – 1 m/s					
	12,159	466.741	454.669	12.072	2.59
	10,803	468.425	456.188	12.237	2.61
	11,980	470.802	459.602	11.200	2.38
roughness 0.5 mm	13,730	473.810	461.440	12.370	2.61
Smooth	13,685	471.239	459.928	11.311	2.40
Flow velocity – 10 m/s					
	133,940	46,808.8	45,702.3	1,106.5	2.36
	127,800	46,751.1	45,654.1	1,097.0	2.35
	130,560	47,079.8	46,020.3	1,059.5	2.25
	141,720	46,625.0	45,664.6	960.4	2.06
	141,670	46,567.0	45,638.5	928.5	1.99
	142,500	46,698.4	45,810.8	887.6	1.9
Smooth	150,010	47,063.6	46,037.6	1,026.0	2.18
roughness 0.5 mm	113,720	50,561.9	48,766.5	1,161.3	2.45

Table-2 indicates that scales with a flow separation area are largely inferior to scales with a shank. Aside from that, we can note that pressure losses in the flow around the plate with an equivalent roughness of 0.5 mm are approximately the same as with plates having scales with a separation zone. The location of the ridge top along the scale length also has some effect on the formation of a boundary layer in a turbulent flow and the amount of flow energy loss.

The shears of velocity distribution in the flow around plates with sharkskin imitation demonstrate that part of the flow energy is spent on the formation of

vortices behind the scales, thereby increasing vortex losses. The degree of vortex formation largely depends on the geometry of the element. Scales with shanks do not have this disadvantage.

Several similar experiments were conducted to determine the mutual influence of the positioning of scales on the plate and energy losses in the flow around the plate (Figure-14). In the case of the plate, we considered the options of the double row of scales located at the inlet and outlet edges and in the middle of the plate. The dimensions of the studied plate were: length - 200 mm, width - 20 mm, and thickness - 5 mm.

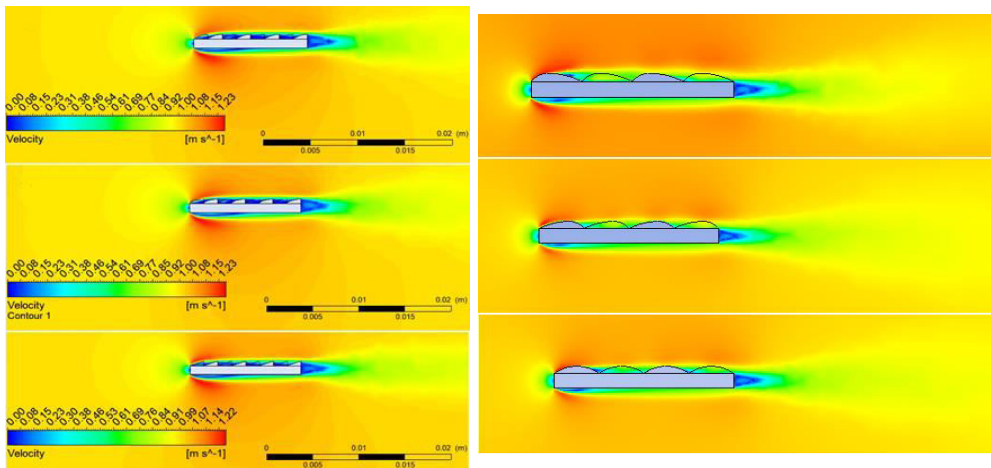


Figure-14. Flow velocity distribution in the longitudinal section in the flow around the modified plates.

The experiments with plates suggest that the most efficient option is the sharkskin imitation located at the inlet edge because this area has the most turbulent flow (Figure-15). This option reduces the losses of full pressure by 5.4% compared to the smooth control plate with a Reynolds number of about 90,000 and with $Re=900,000$ - by 3.9%.

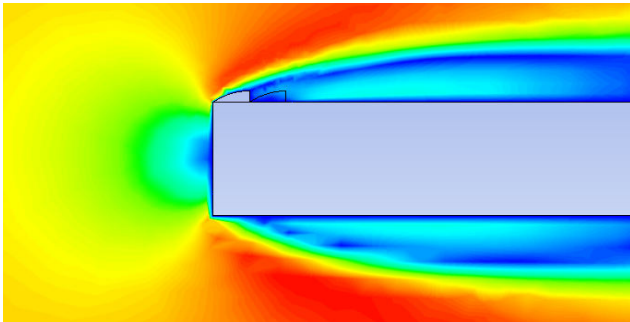


Figure-15. Velocity distribution in the flow around the inlet edge of the plate.

Velocity profiles in the wake behind the plate at distances of 20, 30, and 40 mm from the inlet edge for the physical experiment and computer modeling (Figure-16) demonstrate that the results obtained on the flow around the modified plates are sufficiently reliable.

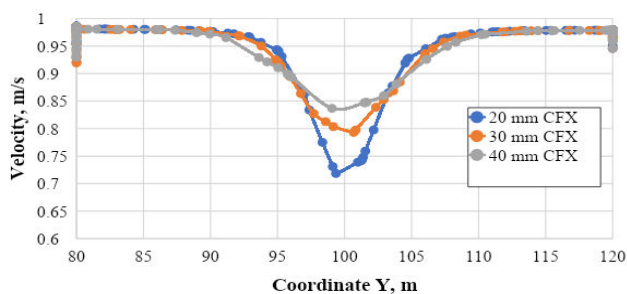


Figure-16. Velocity profiles in the wake behind the plate at distances of 20, 30, and 40 mm.

Thus, our study on hydrodynamic effects based on biomimicry for technical systems indicates that current research focuses on raising the ECE. Improvement of the ECE can be attained through modification of the working surfaces interacting with the flow in the near-wall area, thereby reducing hydraulic drag as fluid flows around the object. The majority of biomimetic surfaces are proposed for use in the automotive, aircraft, and shipbuilding industries.

The study confirms that at present, the scientific world has not reached a unanimous opinion on the mechanisms of influence of nature-like surface microstructure on the flow in the near-wall area, as well as the reasons behind the reduction of hydraulic drag.

CONCLUSIONS

The study of sharkskin morphology demonstrates that in fast-swimming sharks, the angle of attack of scales relative to the skin surface is dependent on the speed of movement - the greater the speed, the more the scales of sharkskin protrude, increasing the level of attack against the flow.

Computational studies of the change in the hydraulic drag show that the positive hydrodynamic effect of sharkskin reduced the drag of a body in a liquid medium by 5 to 25%, depending on the shape and nature of the movement of the body, as well as on the method of simulating sharkskin.

Despite the great promise of using the sharkskin effect in technical systems, there are no recorded variants of its use in vane pumps or hydraulic turbines. Therefore, research into the use of nature-inspired methods of modification of flow part elements of hydromachines presents a topical task.

ACKNOWLEDGEMENTS

The research was supported by the grant of the President of the Russian Federation for state support of young Russian scientist candidates of technical sciences "Study of the influence of modification of functional surfaces of hydraulic machines by the principles of



biomimetics on hydraulic losses" (Agreement No. 075-15-2022-730 of May 17, 2022, internal number MK-4548.2022.4).

CREDIT AUTHORSHIP CONTRIBUTION STATEMENT

Author 1: Methodology, Investigation, Funding Acquisition. Author 2: Formal analysis. Author 3: Methodology, Formal Analysis, Supervision. Author 4: Investigation, Formal analysis. Author 5: Methodology, Investigation.

DECLARATION OF COMPETING INTEREST

The authors declare that they have no known competing financial interests or personal relationships that could have appeared to influence the work reported in this paper.

REFERENCES

- [1] Ministry of Energy of the Russian Federation. Main characteristics of the Russian electric power industry. <https://minenergo.gov.ru/node/532>
- [2] The benefits of sliding vane pump technology. 2019. *World Pumps*. 2019(3): 38-42. [https://doi.org/10.1016/S0262-1762\(19\)30039-2](https://doi.org/10.1016/S0262-1762(19)30039-2)
- [3] Banaś M. 2021. Volumetric efficiency of a hydraulic pump with plastic gears working with tap water, In: J. Stryczek and U. Warzyńska (eds) *Advances in Hydraulic and Pneumatic Drives and Control 2020. NSHP 2020. Lecture Notes in Mechanical Engineering*, pp. 355-366. Springer, Cham. https://doi.org/10.1007/978-3-030-59509-8_32
- [4] Jasiński R. 2021. Volumetric and torque efficiency of pumps during start-up in low ambient temperatures, In: J. Stryczek and U. Warzyńska (eds) *Advances in Hydraulic and Pneumatic Drives and Control 2020. NSHP 2020. Lecture Notes in Mechanical Engineering*, pp. 28-39. Springer, Cham. https://doi.org/10.1007/978-3-030-59509-8_3
- [5] Sliwinski P. and Patrosz P. 2021. The influence of water and mineral oil on pressure losses in hydraulic motor, In: J. Stryczek and U. Warzyńska (eds) *Advances in Hydraulic and Pneumatic Drives and Control 2020. NSHP 2020. Lecture Notes in Mechanical Engineering*, pp. 112-122. Springer, Cham. https://doi.org/10.1007/978-3-030-59509-8_10
- [6] Yang F., Zhao H-r. and Liu C. 2016. Improvement of the efficiency of the axial-flow pump at part loads due to installing outlet guide vanes mechanism. *Mathematical Problems in Engineering*. 2016: 6375314. <http://dx.doi.org/10.1155/2016/6375314>
- [7] Liu H., Cheng Z., Ge Z., Dong L. and Dai C. 2021. Collaborative improvement of efficiency and noise of bionic vane centrifugal pump based on multi-objective optimization. *Advances in Mechanical Engineering*. 13(2): 1-13. <https://doi.org/10.1177/1687814021994976>
- [8] Tian Y., Hu A. and Zheng Q. 2020. The effect of guide vane type on the performance of multistage energy recovery hydraulic turbine (MERHT). *Open Physics*. 18(1): 352-364. <https://doi.org/10.1515/phys-2020-0141>
- [9] Afroz F., Lang A., Habegger M. L., Motta P. and Hueter R. 2016. Experimental study of laminar and turbulent boundary layer separation control of shark skin. *Bioinspiration & Biomimetics*. 12: 016009. <https://doi.org/10.1088/1748-3190/12/1/016009>
- [10] Biomimetics. <https://www.nature.com/subjects/biomimetics>.
- [11] Martin S. and Bhushan B. 2016. Modeling and optimization of shark-inspired riblet geometries for low drag applications. *Journal of Colloid and Interface Science*. 474: 206-215. <https://doi.org/10.1016/j.jcis.2016.04.019>
- [12] Guo P., Zhang K., Yasuda Y., Yang W., Galipon J. and Rival D. E. 2021. On the influence of biomimetic shark skin in dynamic flow separation. *Bioinspiration & Biomimetics*. 16: 034001. <https://doi.org/10.1088/1748-3190/abdf31>
- [13] Kim T. W. 2014. Assessment of hydro/oleophobicity for shark skin replica with riblets. *Journal of Nanoscience and Nanotechnology*. 14(10): 7562-7568. <https://doi.org/10.1166/jnn.2014.9570>
- [14] Lu Y., Hua M. and Liu Z. 2014. The biomimetic shark skin optimization design method for improving lubrication effect of engineering surface. *Journal of Tribology*. 6(3): 031703. <https://doi.org/10.1115/1.4026972>
- [15] Qin L., Hafezi M., Yang H., Dong G. and Zhang Y. 2019. Constructing a dual-function surface by microcasting and nanospraying for efficient drag reduction and potential antifouling capabilities. *Micromachines*. 10(7): 490. <https://doi.org/10.3390/mi10070490>



- [16] Ankhelyi M. V., Wainwright D. K. and Lauder, G. V. 2018. Diversity of dermal denticle structure in sharks: skin surface roughness and three-dimensional morphology. *Journal of Morphology*. 279(8): 1132-1154. <https://doi.org/10.1002/jmor.20836>
- [17] Lauder G. V., Wainwright D. K., Domel A. G., Weaver J. C. and Bertoldi L. W. K. 2016. Structure, biomimetics, and fluid dynamics of fish skin surfaces. *Physical Review Fluids*. 1: 060502. <https://doi.org/10.1103/PhysRevFluids.1.060502>
- [18] Martin S. and Bhushan B. 2016. Discovery of riblets in a bird beak (Rynchops) for low fluid drag. *Philosophical Transactions of the Royal Society A: Mathematical, Physical and Engineering Sciences*. 374(2073): 20160134. <https://doi.org/10.1098/rsta.2016.0134>
- [19] Pu X., Li G. and Huang H. 2016. Preparation, anti-biofouling and drag-reduction properties of a biomimetic shark skin surface. *Biology Open*. 5(4): 389-396. <https://doi.org/10.1242/bio.016899>
- [20] Chen D., Liu Y., Chen H. and Zhang D. 2018. Bio-inspired drag reduction surface from sharkskin. *Biosurface and Biotribology*. 4: 39-45. <https://doi.org/10.1049/bsbt.2018.0006>
- [21] Daehne B. and Watermann B. 2012. Shark skin morphology and hydrodynamic properties. *Special Greentech. Surface Technology*, pp. 48-50. Ship & Offshore, GreenTech.
- [22] Wen L., Weaver J. C. and Lauder G. V. 2014. Biomimetic shark skin: Design, fabrication and hydrodynamic function. *Journal of Experimental Biology*. 217(10): 1656-1666. <https://doi.org/10.1242/jeb.097097>
- [23] Ibrahim M. D., Amran S. N. A., Yunus Y. S., Rahman M. R. A., Mohtar M. Z., Wong L. K. and Zulkharnain A. 2018. The study of drag reduction on ships inspired by simplified shark skin imitation. *Applied Bionics and Biomechanics*. 2018: 7854321. <https://doi.org/10.1155/2018/7854321>
- [24] Liu C., Meng H., Lu S., Li A., Xu, C., Sun Y. and Wang G. 2022. Design of nonsmooth groove tire bioinspired by shark-skin riblet structure. *Applied Bionics and Biomechanics*. 2022: 6025943. <https://doi.org/10.1155/2022/6025943>
- [25] Wen L., Weaver, J. C., Thornycroft, P. J. M. and Lauder G. V. 2015. Hydrodynamic function of biomimetic shark skin: Effect of denticle pattern and spacing. *Bioinspiration & Biomimetics*. 10(6): 066010. <https://doi.org/10.1088/1748-3190/10/6/066010>
- [26] Domel A. G., Domel G., Weaver J. C., Saadat M., Bertoldi K. and Laude G. V. 2019. Hydrodynamic properties of biomimetic shark skin: Effect of denticle size and swimming speed. *Bioinspiration & Biomimetics*. 13(5): 056014. <https://doi.org/10.1088/1748-3190/aad418>
- [27] ANSYS Inc., Ansys Fluids Computational Fluid Dynamics (CFD) Simulation Software. 2022. <https://www.ansys.com>